AIP Applied Physics Letters

Self-induced spin-polarized carrier source in active photonic device with artificial optical chirality

Yuqian Ye and Shu-Wei Chang

Citation: Applied Physics Letters **101**, 181106 (2012); doi: 10.1063/1.4765082
View online: http://dx.doi.org/10.1063/1.4765082
View Table of Contents: http://scitation.aip.org/content/aip/journal/apl/101/18?ver=pdfcov
Published by the AIP Publishing

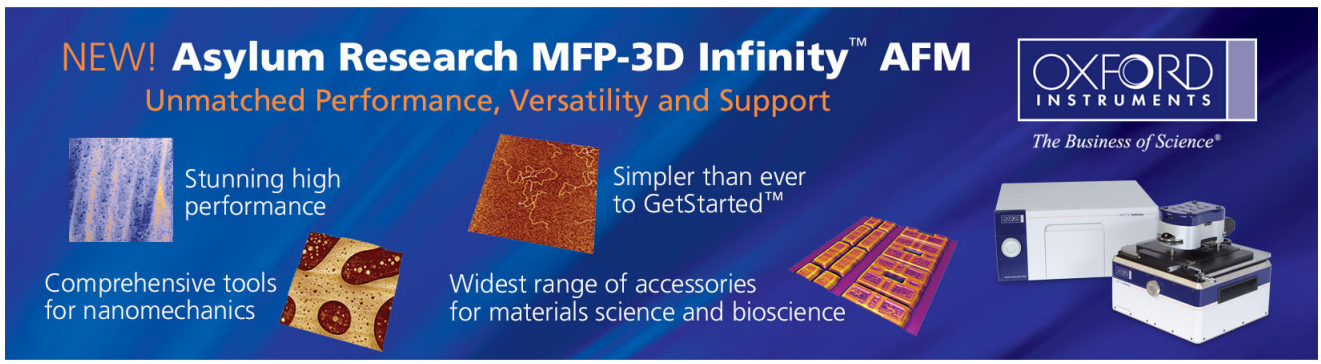

Self-induced spin-polarized carrier source in active photonic device with artificial optical chirality

Yuqian Ye[1,2] and Shu-Wei Chang[1,3,a)]
[1]*Research Center for Applied Sciences, Academia Sinica, Nankang, Taipei 11529, Taiwan*
[2]*Department of Physics, Hangzhou Normal University, Hangzhou, Zhejiang 310012, China*
[3]*Department of Photonics, National Chiao-Tung University, Hsinchu 30010, Taiwan*

(Received 13 September 2012; accepted 17 October 2012; published online 29 October 2012)

We demonstrate a scheme of active photonic devices which can spontaneously polarize the carrier spin in active regions. Rather than externally breaking the time-reversal symmetry of carrier spin states such as applying magnetic fields, only the optical chirality is required in this setup. Spin-polarized carriers are generated by interactions between carriers and self-initiated circularly polarized photons without the spin-selective optical pumping/electrical injection and breaking of the reciprocity. The device requires a cavity which supports modes with only one circular polarization and can be implemented with the vertical-cavity type of arrangements for distributed Bragg reflectors and artificial chiral photonic structures. © *2012 American Institute of Physics*. [http://dx.doi.org/10.1063/1.4765082]

The electron spin can store and carry information in addition to the charge.[1] For this purpose, the generation of spin-polarized (SP) carriers in semiconductors is important in spintronics. Electronics-wise, this process requires SP carrier injections through ferromagnetic materials and external magnetic fields,[2–6] which marks the broken time-reversal (T) symmetry of carrier spin states. However, the Curie temperature of compatible magnetic injectors, above which the spontaneous magnetization vanishes, is often below room temperature[7] and limits related applications.

Characteristics of bandedge states in III-V semiconductor nanostructures provide another route to SP carriers through optical pumping.[8] The momentum selection rules indicate that the absorption of circularly polarized (CP) photons creates carriers in a specific spin (angular momentum) state.[9,10] Still, the induced spin polarization is usually nonpersistent at room temperature. Alternatively, a perspective to the issue is whether carriers of a certain spin species in an initially unpolarized ensemble can be forced to rapidly emit CP photons so that the spin polarization is self-maintained. Namely, we are seeking active photonic devices in which spontaneous spin polarizations are induced under spin-nonselective electrical injections without the imposed T-symmetry breaking.

Optical chirality, which distinguishes two circular polarizations in a time-reversible (reciprocal) way, may be the key to the device. Chiral objects cannot be superimposed on their mirror images and respond to two CP fields distinctly. Utilizing this feature, we can construct cavities which only support cavity modes with a particular circular polarization.[11] With such a cavity that favors CP modes spinning, for example, clockwise (photon spin quantum number $m_{s,ph} = -1$) around the growth direction of a typical quantum well (QW) in Fig. 1, optical feedback channels are altered. If stimulated emissions into these modes dominate, selection rules ensure that only the spin-up electrons coherently emit CP photons with $m_{s,ph} = -1$ and recombine with quasi-equilibrium holes in the heavy-hole state $|3/2, 3/2\rangle$. Thus, the stimulated emissions clamp spin-up electron density $n_\uparrow$ but leave the other $n_\downarrow$ intact. Both spin species recombine via other mechanisms with a lifetime τ. However, once the stimulated emission rate exceeds the spin relaxation rate τ_s^{-1}, an observable spin polarization of electrons is induced. In fact, the spinning field of stimulated photons is just a spin pump which continuously transfers the spin angular momentum of electrons out of the cavity.

Polarization-dependent phenomena in chiral photonic structures are important in applications and sciences. For example, cholesteric liquid crystals (CLCs) are utilized in active CP photon sources.[12–15] Recent attention has been put on chiral metamaterials related to the negative refractive index[16,17] and giant optical activity.[18,19] Three-dimensional (3D) chiral photonic crystals which show similar features as those of CLCs have also been realized.[20–24] With these chiral structures, our goal is to demonstrate aforementioned cavities as spin pumps. Despite challenging fabrications, we focus on 3D artificial chiral structures since they are potentially adjustable for infrared (IR) wavelengths such as

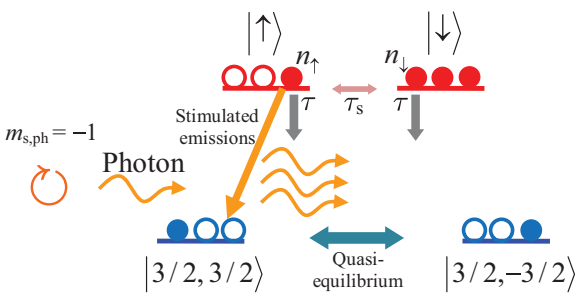

FIG. 1. Transitions between bandedge states in a QW. Due to the selection rules, only the spin-up carriers are clamped by stimulated emissions of photons with $m_{s,ph} = -1$.

a)Electronic mail: swchang@sinica.edu.tw.

telecommunication ones near 1.3 and 1.55 μm, while CLCs are limited to visible and near-IR ranges shorter than 0.85 μm.[25]

The spinning field inside active regions is important for spin pumps because linearly polarized (LP) photons do not distinguish spin states. Circularly polarized fields solely outside cavities are also unhelpful. It happens that typical CLC bandedge and defect lasing modes are spatially helical but linearly polarized inside cavities.[14] Hence, scheme modifications are necessary for artificial chiral structures similar to CLCs. Later, we will show that combinations of distributed Bragg reflectors (DBRs) and 3D artificial chiral structures can serve the purpose.

We use rate equations to describe the working principle of the spin pump

$$\frac{\partial n_\sigma}{\partial t} = \frac{\eta_i I}{2qV_a} - \frac{n_\sigma}{\tau} - \frac{(n_\sigma - n_{\bar\sigma})}{\tau_s} - v_g g_\sigma S, \tag{1a}$$

$$\frac{\partial S}{\partial t} = -\frac{S}{\tau_p} + \Gamma \sum_\sigma \left(\frac{\beta_{sp,\sigma} n_\sigma}{\tau_{sp}} + v_g g_\sigma S \right), \tag{1b}$$

where σ and $\bar\sigma$ $(=\uparrow,\downarrow)$ are the spin index and its counterpart; I and η_i are the spin-nonselective injection current and injection efficiency; q is the electron charge; V_a is the volume of the active region; v_g is the group velocity; S, Γ, and τ_p are the photon density, confinement factor, and photon lifetime of the spinning mode; τ_{sp} is the spontaneous-emission lifetime; and $\beta_{sp,\sigma}$ and g_σ are the spin-dependent spontaneous emission coupling factor and gain. In Eq. (1a), the third term characterizes the spin relaxation, and in Eq. (1b), we adopt spin-independent lifetimes τ_{sp} and τ, which is valid for reciprocal environments[11] and assumed approximately correct here. The spin-dependent gain g_σ is modeled as $g_\sigma = \gamma_\sigma a(2n_\sigma - n_{tr})$, where γ_σ are factors dependent on the mode polarization and band mixing near the QW bandedge, a is the differential gain, and n_{tr} is the transparency carrier density. If the mode polarization is close to that indicated in Fig. 1, parameters γ_σ satisfy the condition $\gamma_\uparrow \approx 1 \gg \gamma_\downarrow$. On the other hand, for LP modes, we have $\gamma_\uparrow = \gamma_\downarrow = 0.5$ and $\beta_{sp,\uparrow} = \beta_{sp,\downarrow}$, and summing the two rate equations of $n_\uparrow$ and $n_\downarrow$ in Eq. (1a) recovers the usual one for the total carrier density.

Although some parameters in Eqs. (1a) and (1b) are density-dependent, we adopt typical values near thresholds of QW lasers for simplicity. Except for τ_s, other parameters are fixed as follows: $\tau_{sp} = 3$ ns, $\tau = 2.5$ ns, $\tau_p = 2.5$ ps, $\Gamma = 0.05$, $v_g = c/4$ (c is the vacuum speed of light), $a = 5 \times 10^{-16}$ cm^2, $n_{tr} = 1.5 \times 10^{18}$ cm^{-3}, $\gamma_\uparrow = 0.999$, $\gamma_\downarrow = 10^{-3}$, and $\beta_{sp,\uparrow} = \beta_{sp,\downarrow} = 2 \times 10^{-4}$. The steady-state solutions to Eqs. (1a) and (1b) are then solved self-consistently. In Figs. 2(a) and 2(b), we show carrier densities $n_\uparrow$ and $n_\downarrow$, respectively, as a function of the injection current I for different τ_s (properly scaled). While $n_\uparrow$ is pinned by the stimulated emission above a threshold current, $n_\downarrow$ is unaffected by the feedback process and can be built up as long as spin is not flipped rapidly (long τ_s). The density $n_\uparrow$ seems nearly unrelated to τ_s, but the photon density S [Fig. 2(c)] does become higher as τ_s turns shorter because $n_\downarrow$ may replenish spin-up carriers when the spin relaxation is fast. On the other hand, as indicated in Fig. 2(d) with $\tau_s \lesssim 0.1$ ns, which is common for [001] QWs at room temperature,[26] the degree of spin polarization (DSP) defined as $|n_\uparrow - n_\downarrow|/(n_\uparrow + n_\downarrow)$ is only a few percents (or even fewer) at a high injection rate. Under such circumstances, the longer photon lifetime and larger differential gain may be required so that the even higher stimulated emission rate can induce the more spin polarization at the same injection level. Alternatively, [110] QWs with a room-temperature τ_s in the nanosecond range could be helpful.[27] If a DSP close to unity is required, the carriers providing the gain to the spinning mode (unwanted spin species) and nonradiative recombination rate impeding the accumulation of spin-polarized carriers at a high injection level also have to be reduced.

Cavities that only support modes with a certain circular polarization are most critical to optical spin pumps. The implementation is based on the two co-rotating elliptical polarization eigenstates of an artificial chiral reflector, which

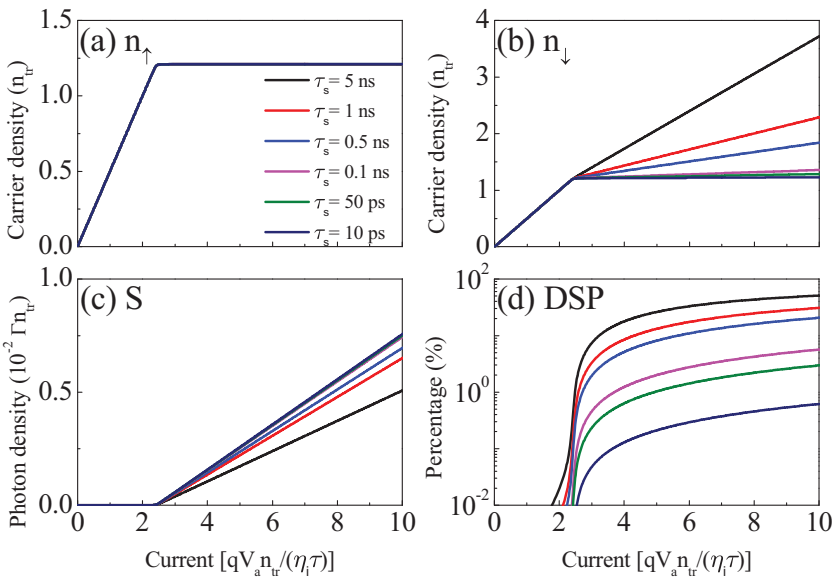

FIG. 2. (a) The spin-up carrier density, (b) spin-down counterpart, (c) photon density, and (d) degree of spin polarization as a function of the injection current under different τ_s (logarithmic scale). While $n_\uparrow$ is pinned by stimulated emissions, $n_\downarrow$ can be built up with a sufficiently long τ_s. If τ_s is longer, DSP becomes larger, but S turns slightly lower.

are both close to a particular circular polarization.[11] Denote the growth direction of QWs as $\hat{z}$ and define the counter-clockwise/clockwise circular polarizations around $\hat{z}$ as $\hat{e}_{\pm} \equiv (\hat{x} \pm i\hat{y})/\sqrt{2}$. The reflection matrix $\mathbf{r}_{\mathrm{CP}}$ of the chiral reflector in CP bases is

$$\mathbf{r}_{\mathrm{CP}} = \begin{pmatrix} r_{++}, & r_{+-} \\ r_{-+}, & r_{--} \end{pmatrix}. \tag{2}$$

The reciprocity requires $r_{++} = r_{--}$,[28] and eigenstates and eigenvalues of $\mathbf{r}_{\mathrm{CP}}$ then become[11,29]

$$\mathbf{w}_{1,2} = \frac{\sqrt{|r_{-+}|}}{\sqrt{|r_{+-}| + |r_{-+}|}} \begin{pmatrix} \pm\sqrt{r_{+-}/r_{-+}} \\ 1 \end{pmatrix}, \tag{3a}$$

$$\Lambda_{1,2} = r_{++} \pm \sqrt{r_{+-} r_{-+}}. \tag{3b}$$

If we design the reflector so that $|r_{+-}/r_{-+}|^{1/2} \ll 1$, the two polarization eigenstates $\mathbf{w}_{1,2}$ in Eq. (3a) both resemble $\hat{e}_-$. These polarization states are then singled out through the Fabry-Perot (FP) resonances in a resonator arrangement of DBRs and this chiral reflector similar to the layout of vertical-cavity surface-emitting lasers.

We construct such reflectors by cascading a DBR and 3D chiral structure in series. Although 3D chiral structures alone exhibit the feature $|r_{+-}/r_{-+}|^{1/2} \ll 1$, their magnitudes $|r_{++}|$ ($|r_{--}|$) are low and lead to small reflectivies $|\Lambda_{1,2}|^2$ of the polarization eigenstates. This phenomenon significantly increases the lasing threshold of the cavity to be constructed. The purpose of the DBR insertion is to boost up the magnitudes $|r_{++}|$ and $|\Lambda_{1,2}|^2$.[11] More DBR layers enhance $|r_{++}|$ up to unity. On the other hand, while a thick DBR does not alter the ratio $|r_{+-}/r_{-+}|$ originating from 3D chiral structures much, the magnitudes $|r_{+-}|$ and $|r_{-+}|$ do drop with the layer number. In this case, the chirality is more sensitive to fluctuations, which is a trade-off.

Limited by computation resources, we do not model 3D structures with many alternate layers and repeated units in the near-IR range. Rather, with a few layers/units, we demonstrate prototypes of the reflector and cavity in the mid-IR window based on high-contrast DBRs and metallic helices that exhibit prominent optical responses in this frequency range.[30] The corresponding semiconductor gain media are superlattices designed for mid-IR interband quantum cascade lasers.[31] The implementation in the near-IR range follows similar design rules. A unit cell of the chiral reflector is shown in Fig. 3(a). It consists of DBR layers with alternate refractive indices $n_1 = 2.8$ and $n_2 = 1.6$ and a 3-pitch gold helix with the pitch height $p = 3.5\,\mu$m, radius $r = 0.31\,\mu$m, and wire diameter $d = 0.12\,\mu$m. The lattice constant a of the cell is $1.1\,\mu$m. The permittivity of gold is modeled by the Drude model.[32]

The magnitudes of reflection coefficients as a function of frequency are shown in Fig. 3(b). The calculations are carried out with the commercial software COMSOL. The gray region (67.6 to 85.5 THz) is the chiral stop band of the gold helix array. From these spectra, $|r_{-+}|$ ranges from 0.05 to 0.15 in the chiral stop band while $|r_{+-}|$ is vanishingly small. The magnitude ratio $|r_{+-}/r_{-+}|$ remains less than 0.03 in this frequency range, indicating that two polarization eigenstates should resemble $\hat{e}_-$. The yellow region (70 to 100 THz) in Fig. 3(b) represents the photonic band gap of DBR, which is designed to overlap with the chiral stop band and boosts up $|r_{++}|$ (identical to $|r_{--}|$ due to reciprocity).

Based on this chiral reflector, we construct the cavity with a unit cell shown in Fig. 4(a). Another DBR similar to that mentioned previously is placed at the left side of the chiral reflector. The two reflectors are separated by a semiconductor layer (active region) with a refractive index $n_a = 3.4$ and length $l = 6.1\,\mu$m. The whole structure forms a FP cavity. The magnitudes of reflection coefficients versus frequency for waves incident from the left of the cavity are shown in Fig. 4(b). Sharp resonance peaks ($|r_{-+}|$) and resonant dips ($|r_{++}|$) inside the DBR stop band [yellow region in Fig. 3(b)] correspond to FP modes. As an example, the reflection spectra of the FP mode around the resonance frequency $f_0 = 73.82\,\mathrm{THz}$ [$\lambda_0 = c/f_0 = 4.06\ \mu$m, marked with $*$ in Fig. 4(b)] are shown in Fig. 4(c). The $\hat{e}_-$-polarized incident wave exhibits a resonant transmission featured by the small magnitudes of $|r_{+-}|$ and $|r_{--}|$ near the resonance, while the $\hat{e}_+$-polarized wave is almost reflected with its polarization converted to $\hat{e}_-$. Therefore, we can infer from the transmission (reflection) of $\hat{e}_-$- ($\hat{e}_+$-) polarized waves that FP resonant modes with polarizations close to $\hat{e}_-$ ($m_{\mathrm{s,ph}} = -1$) are excited inside the cavity regardless of incident polarizations. The dashed curve in Fig. 4(c) is the total reflectivity $|r_{+-}|^2 + |r_{--}|^2$ of the $\hat{e}_-$-polarized incident wave. From the dip linewidth, the quality factor of this FP mode is estimated as 211.

The foregoing calculations indirectly indicate the presence of $\hat{e}_-$-like modes. However, as a spin pump, the spinning field has to be self-initiated by carriers in the active region without CP incident waves. To ensure that modes, for

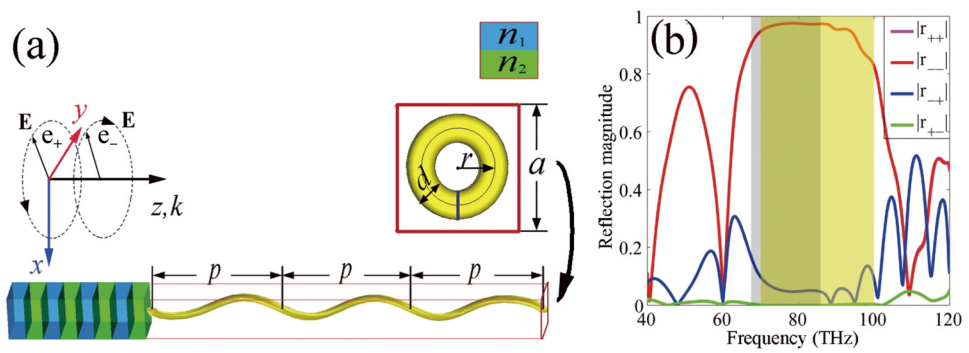

FIG. 3. (a) The unit cell of the chiral reflector composed of a DBR and gold helix. The inset shows the front view of a gold helix. (b) The magnitudes of reflection coefficients versus frequency. The yellow region is the DBR stop band.

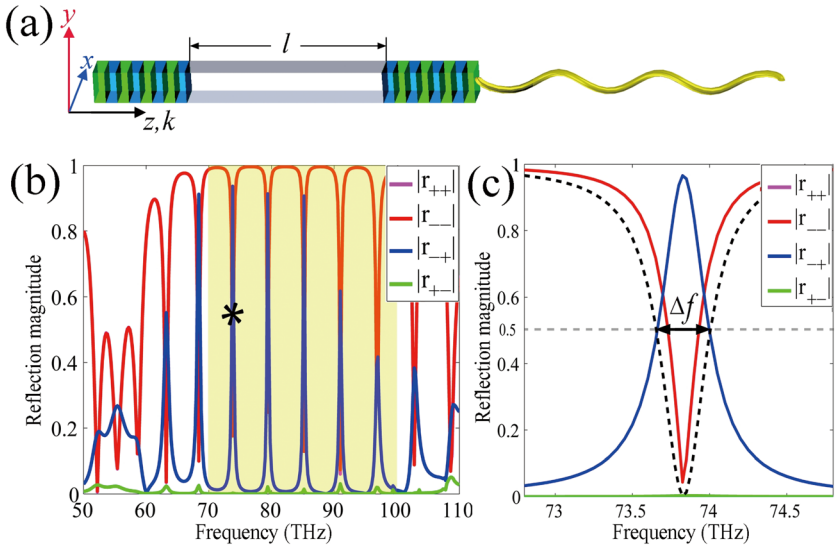

FIG. 4. (a) The unit cell of the cavity is composed of a DBR and the chiral reflector. (b) The magnitudes of reflection coefficients versus frequency for waves incident from the left of the cavity. The mark $*$ indicates the resonance at $f_0 = 73.82$ THz. (c) The spectra near f_0. The dashed curve is the total reflection $|r_{+-}|^2 + |r_{--}|^2$ of the $\hat{e}_-$-polarized incident wave.

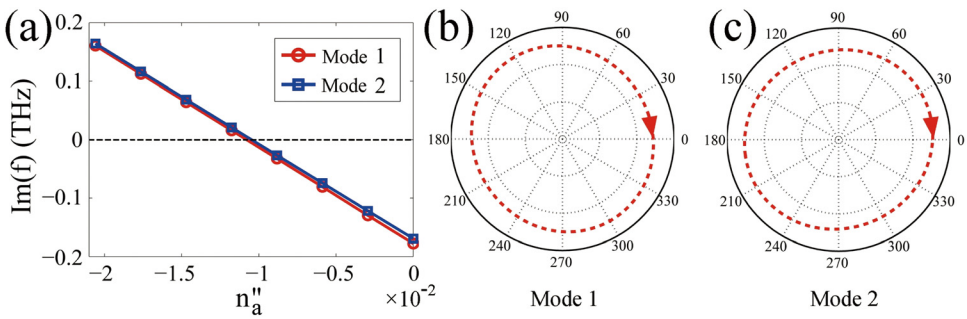

FIG. 5. (a) The two imaginary parts of the eigenfrequencies versus n_a''. They nearly vanish around $n_a'' = -1.05 \times 10^{-2}$. (b) The polarization pattern of mode 1, and (c) the counterpart of mode 2. Both polarizations resemble $\hat{e}_-$.

instance, near f_0 all have polarizations close to $\hat{e}_-$, we solve the 3D complex eigenfrequency problem with outgoing-wave boundary conditions and inspect polarization patterns of the obtained eigenmodes. The material gain $g \approx -4\pi f_0 n_a''/c$ that models the initially spin-unpolarized ensemble of carriers is introduced through the imaginary part n_a'' of the semiconductor refractive index. For different n_a'', we obtain two eigenmodes of which the real parts of their eigenfrequencies $\mathrm{Re}[f_1] \approx 73.82$ THz (mode 1) and $\mathrm{Re}[f_2] \approx 73.83$ THz (mode 2) are close to each other and do not vary much with n_a''. These two eigenmodes correspond to two polarization eigenstates $\mathbf{w}_{1,2}$ of the chiral reflector [Eq. (3a)]. The imaginary parts of the two eigenfrequencies $\mathrm{Im}[f_1]$ and $\mathrm{Im}[f_2]$ versus n_a'' are illustrated in Fig. 5(a). As n_a'' reaches around -1.05×10^{-2} ($g = 3.25 \times 10^2\,\mathrm{cm}^{-1}$), both imaginary frequencies almost vanish, namely, these two FP modes start to lase. The polarization patterns of the two lasing modes inside the cavity are shown in Figs. 5(b) and 5(c). The two polarizations rotate clockwise around the $\hat{z}$ direction with an ellipticity of 1.07. This number corresponds to a degree of circular polarization DCP $\equiv |I_+ - I_-|/(I_+ + I_-) \approx 99.8\%$, where $I_\pm$ are square magnitudes of $\hat{e}_\pm$ components in these modes. No matter which mode dominates in lasing, the polarization of stimulated emitted photons is always close to $\hat{e}_-$. In this way, the majority of spin-down electrons do not participate in photon multiplications and can accumulate in active regions. However, the usual DSP estimation based on DCP of photons from QWs is not a confirmation of the spin polarization here because the chiral structure itself is a CP filter. To avoid the interference, measurements of the polarization rotation and nonreciprocity of probes propagating along the QW plane due to the Voigt effect from SP carriers, though challenging, can be utilized.

In summary, we demonstrate a scheme of active photonic devices which induce SP carriers in active regions. Neither explicit breaking of the T symmetry of spin states and reciprocity of optical fields nor spin-selective optical pumpings/electrical injections are necessary. The functionality requires that polarizations of cavity modes resemble one particular circular polarization in active regions. The CP-like cavity modes function as spin pumps when the stimulated emission rate exceeds spin relaxation rate. The cavity could be constructed with artificial chiral photonic structures.

This work was sponsored by Research Center for Applied Sciences, Academia Sinica, Taiwan, and National Science Council, Taiwan, under Grant No. NSC100-2112-M-001-002-MY2. Y. Ye also appreciates the partial support from National Natural Science Foundation of China under Project No. 61201115.

[1]I. Žutić, J. Fabian, and S. Das Sarma, Rev. Mod. Phys. **76**, 323 (2004).
[2]M. Johnson and R. H. Silsbee, Phys. Rev. Lett. **55**, 1790 (1985).
[3]Y. Ohno, D. K. Young, B. Beschoten, F. Matsukura, H. Ohno, and D. D. Awschalom, Nature **402**, 790 (1999).
[4]A. T. Hanbicki, B. T. Jonker, G. Itskos, G. Kioseoglou, and A. Petrou, Appl. Phys. Lett. **80**, 1240 (2002).
[5]X. Jiang, R. Wang, S. van Dijken, R. Shelby, R. Macfarlane, G. S. Solomon, J. Harris, and S. S. P. Parkin, Phys. Rev. Lett. **90**, 256603 (2003).

[6]M. Holub, J. Shin, D. Saha, and P. Bhattacharya, Phys. Rev. Lett. **98**, 146603 (2007).
[7]T. Jungwirth, K. Y. Wang, J. Mašek, K. W. Edmonds, J. König, J. Sinova, M. Polini, N. A. Goncharuk, A. H. MacDonald, M. Sawicki, A. W. Rushforth, R. P. Campion, L. X. Zhao, C. T. Foxon, and B. L. Gallagher, Phys. Rev. B **72**, 165204 (2005).
[8]F. Meier and B. P. Zakharchenya, *Optical Orientation* (North-Holland, Amsterdam, 1984).
[9]H. Ando, T. Sogawa, and H. Gotoh, Appl. Phys. Lett. **73**, 566 (1998).
[10]H. Fujino, S. Koh, S. Iba, T. Fujimoto, and H. Kawaguchi, Appl. Phys. Lett. **94**, 131108 (2009).
[11]S. W. Chang, Opt. Express **20**, 2516 (2012).
[12]V. I. Kopp, B. Fan, H. K. M. Vithana, and A. Z. Genack, Opt. Lett. **23**, 1707 (1998).
[13]J. Schmidtke, W. Stille, and H. Finkelmann, Phys. Rev. Lett. **90**, 083902 (2003).
[14]J. Schmidtke and W. Stille, Eur. Phys. J. E **12**, 553 (2003).
[15]J. Hwang, M. H. Song, B. Park, S. Nishimura, T. Toyooka, J. W. Wu, Y. Takanishi, K. Ishikawa, and H. Takezoe, Nature Mater. **4**, 383 (2005).
[16]J. B. Pendry, Science **306**, 1353 (2004).
[17]S. Zhang, Y. S. Park, J. Li, X. Lu, W. Zhang, and X. Zhang, Phys. Rev. Lett. **102**, 023901 (2009).
[18]A. V. Rogacheva, V. A. Fedotov, A. S. Schwanecke, and N. I. Zheludev, Phys. Rev. Lett. **97**, 177401 (2006).
[19]Y. Ye and S. He, Appl. Phys. Lett. **96**, 203501 (2010).
[20]F. Zhang, J. Xu, A. Lakhtakia, S. M. Pursel, M. W. Horn, and A. Wang, Appl. Phys. Lett. **91**, 023102 (2007).
[21]F. Zhang, J. Xu, A. Lakhtakia, T. Zhu, S. M. Pursel, and M. W. Horn, Appl. Phys. Lett. **92**, 111109 (2008).
[22]M. Thiel, G. von Freymann, and M. Wegener, Opt. Lett. **32**, 2547 (2007).
[23]M. Thiel, M. S. Rill, G. von Freymann, and M. Wegener, Adv. Mater. **21**, 4680 (2009).
[24]J. K. Gansel, M. Thiel, M. S. Rill, M. Decker, K. Bade, V. Saile, G. von Freymann, S. Linden, and M. Wegener, Science **325**, 1513 (2009).
[25]P. J. W. Hands, C. A. Dobson, S. M. Morris, M. M. Qasim, D. J. Gardiner, T. D. Wilkinson, and H. J. Coles, Proc. SPIE **8114**, 81140T (2011).
[26]M. W. Wu, J. H. Jiang, and M. Q. Weng, Phys. Rep. **493**, 61 (2010).
[27]Y. Ohno, R. Terauchi, T. Adachi, F. Matsukura, and H. Ohno, Phys. Rev. Lett. **83**, 4196 (1999).
[28]A. L. Shelankov and G. E. Pikus, Phys. Rev. B **46**, 3326 (1992).
[29]C. Menzel, C. Rockstuhl, and F. Lederer, Phys. Rev. A **82**, 053811 (2010).
[30]J. K. Gansel, M. Wegener, S. Burger, and S. Linden, Opt. Express **18**, 1059 (2010).
[31]R. Q. Yang, C. J. Hill, K. Mansour, Y. Qiu, A. Soibel, R. E. Muller, and P. M. Echternach, IEEE J. Sel. Top. Quantum Electron. **13**, 1074 (2007).
[32]M. A. Ordal, L. L. Long, R. J. Bell, S. E. Bell, R. R. Bell, R. W. Alexander, Jr., and C. A. Ward, Appl. Opt. **22**, 1099 (1983).